Energy-saving Capture at Mars via Backward Stable Orbits

Xiangyu Li* and Dong Qiao†
Beijing Institute of Technology, Beijing 100081, Peoples Republic of China

Malcolm Macdonald‡
University of Strathclyde, Glasgow, G1 1XJ, United Kingdom

Nomenclature

a_m	=	semi-major of Mars
e_m	=	eccentricity of Mars
e_s	=	eccentricity of the spacecraft with respect to Mars
f_m	=	true anomaly of Mars
^{f}	=	variables at the periareion moment
^{i}	=	variables at the initial moment
J_E	=	anomaly-dependent integral in the elliptic restricted three-body problem
R	=	distance between the Sun and Mars
r_p	=	periareion distance of the spacecraft
r_p^*	=	lowest periareion distance from the stable sets
$\mathbf{r}_m$	=	position vector of Mars in the rotating frame
$\mathbf{r}_s$	=	position vector of the spacecraft in the rotating frame
$\mathbf{v}_m$	=	position vector of Mars in the rotating frame
$\mathbf{v}_s$	=	position vector of the spacecraft in the rotating frame
v_p	=	periapsis velocity of spacecraft in the rotating frame
v_∞	=	excess velocity of spacecraft with respect to Mars
W_n	=	n-stable sets
x_{p0}	=	initial point in stable sets
x_{pc}	=	capture point (the lowest periareion of the trajectory from the stable sets)
θ	=	orientation angle of the spacecraft
ϵ	=	Kepler energy of the trajectory with respect to Mars
μ	=	mass parameter of Sun-Mars system

*Ph.D. Candidate, School of Aerospace Engineering; lixiangy@bit.edu.cn
†Professor, School of Aerospace Engineering; Key Laboratory of Dynamics and Control of Flight Vehicle; qiaodong@bit.edu.cn (Corresponding Author)
‡Professor of Space Technology, Department of Mechanical & Aerospace Engineering. malcolm.macdonald.102@strath.ac.uk. Associate Fellow AIAA

μ_m = gravitational parameter of Mars

ϖ_{-1}^{n} = target sets with -1-stable motion backward and n-stable motion forward)

Ω = pseudo-potential energy of the circular restricted three-body problem

I. Introduction

The orbit capture, which transfers the spacecraft from the interplanetary trajectory to the target orbit about a celestial body, is a key event in an exploration mission. A low-energy capture strategy, termed ballistic capture, has been developed and applied to lunar transfer, such as Hiten [1] and GRAIL [2]. Such capture exploits the gravitational force of the multi-body system to change the orbit energy of the spacecraft with respect to the target planet from positive to negative.

Ballistic capture is initially found in a certain region called the weak stability boundaries [3]. In [4–6], the geometry of the WSB were studied in detail and applied to ballistic transfers. Significant progress has been made in this field defining the stable sets, providing more regions in the vicinity of the target, or the primary body for the ballistic capture design [7, 8]. The backward stability of motion was introduced and a systematic design method was provided in [9] to find the ballistic capture opportunities in interplanetary transfer. Meanwhile, the connection between ballistic trajectories and transit orbits about the Lagrange points [10], as well as invariant manifolds associated to the periodic orbits in the circular restricted three-body problem (CRTBP), are sought and proven in [11–13], helping in better understanding the properties of ballistic capture. Based on these studies, the ballistic capture in the Earth-Moon system [14–16], the Jovian system [17, 18] and the Sun-Mercury system [19–21] were developed in detail.

The application of ballistic capture to Mars transfer has also been studied in detail [22–25]. Due to the relatively large excess velocity in Earth-Mars transfer, it was found that Hiten-like captures do not exist in the Sun-Mars system [26]. To solve this, Topputo and Belbruno studied a kind of ballistic capture [26], in which the spacecraft is captured into a ballistic trajectory at a large distance from Mars, and then transferred to the desired region without any further maneuvers. The ballistic capture can offer flexible transfer time and lower capture Δv to high altitude orbits, which provides alternative mission design options for Mars missions.

According to the definition of stable set [9], the motion is defined as n-stable if the orbit performs at least n revolutions around the smaller primary P_2 before escaping or impacting on the primary and the initial point belongs to n-stable sets. Likewise, the orbit is said to be $-m$-stable, if it, backward integrated, makes m revolutions with negative orbit energy with respect to the target planet. Otherwise, it belongs to a $-m$ unstable orbit. Fig. 1 shows the example of -1-stable motion and -1-unstable motion. The ballistic capture in [26] takes full advantages of the -1-unstable orbits, which backward integrated make less than one turn about Mars before escape. However, the complementary set under the same condition, or -1-stable orbits have not been considered in detail. These orbits with backward stability

can also be employed for energy-saving capture, providing unique capture opportunities for Mars transfer.

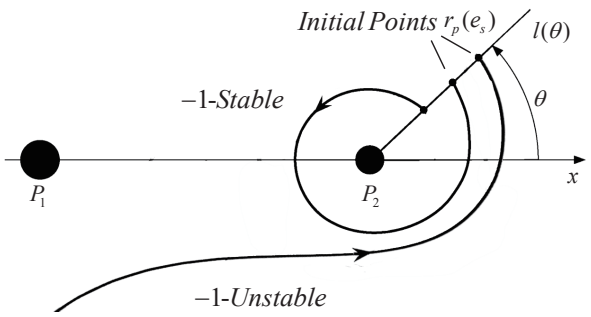

Fig. 1 Example of -1-stable motion and unstable motion

In this Note, we focus on exploiting the backward stable orbits or namely, -1-stable orbits for powered capture at Mars. The capture occurs at the lowest periareion of the backward stable orbits and transits the spacecraft from the interplanetary trajectory to the capture trajectory. Technically, it is not exactly a ballistic capture as a propulsive burn is required. But the capture trajectory has some similar properties as the ballistic capture trajectory that it can transfer naturally to desired regions with prescribed parameters (orbital eccentricity, periareion distant and stability number). In fact, the proposed method changes the position of the capture maneuver from far away Mars in [26] to the periareion.

There are several reasons to use the backward stable orbits and choose the capture maneuver at the periareion. First, if the motion is -1-stable, there might be multiple periareions, which correspond to multiple capture opportunities to the desired regions. Second, the maneuver at periareion usually changes the velocity the most. The periapsis states of the backward stable orbits with respect to Mars will change in each circle, which might provide a better periareion state than the initial state to reduce the capture cost. Third, capture happens within the Sphere of Influence (SOI) of Mars. In that case, any existing methods or techniques for Earth-Mars transfer can be applied. The properties and performance of capture via backward stable orbits are analyzed. The simulation results show that by using the backward stable orbits, more capture opportunities near Mars are available and less capture velocity increment is required compared with direct capture and the capture with -1 unstable motion, especially for high v_∞ and high-altitudes orbit transfer.

II. Dynamical Framework

A. Elliptic Restricted Three-Body Problem

The orbital eccentricity of Mars is $e_m = 0.0934$, which is larger than most of the planets in the solar system. As such, the elliptic restricted three-body problem (ERTBP) is employed in this paper [27]. The ERTBP describes the dynamics of a massless particle, P_3, influenced by two point masses, P_1 and P_2, which revolve around each other in an elliptical orbit, satisfying the condition $m_1 > m_2$. Herein, P_1 is the Sun, P_2 is Mars and P_3 is a spacecraft. The motion

of the spacecraft is established in the rotating barycentric coordinate frame $o-xyz$, as shown in Fig.2. Since the mutual motion of two primaries is elliptic, the coordinate frame rotates non-uniformly. Assuming the normalized length as the semi-major of Mars orbit a_m and normalized time as $T/2\pi$ (T is the orbital period), the normalized equations of motion can be written as [28]

$$\begin{cases} \ddot{x} - 2\omega'\dot{y} - \dot{\omega}'y = \omega'^2 x - \frac{(1-\mu)(x+\mu R)}{r_1^3} - \frac{\mu(x-1+\mu R)}{r_2^3} \\ \ddot{y} + 2\omega'\dot{x} + \dot{\omega}'x = \omega'^2 y - \frac{(1-\mu)y}{r_1^3} - \frac{\mu y}{r_2^3} \\ \ddot{z} = -\frac{(1-\mu)z}{r_1^3} - \frac{\mu z}{r_2^3} \end{cases} \tag{1}$$

where $\mu = m_2/(m_1+m_2)$ is the mass parameter, ω' and $\dot{\omega}'$ are the normalized angular velocity and angular acceleration, $r_1 = \sqrt{(x+R\mu)^2+y^2+z^2}$ and $r_2 = \sqrt{(x-R+R\mu)^2+y^2+z^2}$ are the distance from the spacecraft to the Sun and Mars, respectively. Here R is the distance between the two primaries, which varies with true anomaly of Mars f_m, $R(f_m) = \frac{1-e_m^2}{1+e_m cos f_m}$.

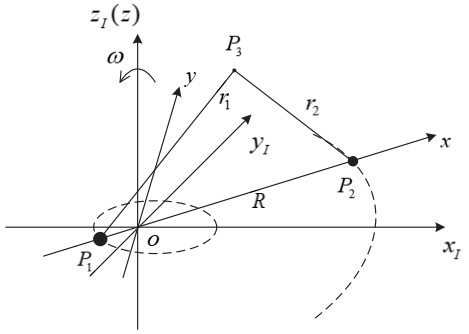

Fig. 2 Coordinate frames and position vectors (the inertial frame $o-x_Iy_Iz_I$; the rotating frame $o-xyz$)

Equation (1) can be transformed to the rotating pulsating coordinate system $O-XYZ$, where the normalized length is chosen as the instantaneous distance of the primary distance. Following [29], the anomaly-dependent integral of motion in the ERTBP reads

$$J_E(f) = 2\Omega - (X'^2+Y'^2+Z'^2) - 2e_m\int_{f_{m0}}^{f_m}\frac{\Omega\sin\tilde{f}}{(1+e_m\cos\tilde{f})^2}d\tilde{f} - 2e_m\int_{f_{m0}}^{f}\frac{Z^2\sin\tilde{f}}{(1+e_m\cos\tilde{f})^2}d\tilde{f} - 2(\Omega+\frac{1}{2}Z^2)\frac{e_m\cos f_m}{1+e_m\cos f_m} \tag{2}$$

where $'$ means the derivative relative to the true anomaly and Ω is the pseudo-potential energy of the circular problem

Note that, the value of J_E depends on both the state of motion and the initial true anomaly of Mars, f_{m0}. If $e_m = 0$, Eq. (2) becomes the Jacobi integral J_C in the circular restricted three-body problem (CRTBP).

B. Integral of Motion with Stable Sets Parameters

The algorithmic definition of the weak stability boundaries (WSB) is introduced in [5]. The stable sets are the extension of the WSB. The formalism of stable sets is introduced in [7, 8], in which stable sets are described as the regions where the spacecraft P_3 can stably orbit about the smaller primary (Mars) P_2 under certain initial conditions. In general, the motion is defined in the xy-plane. The eccentricity of the spacecraft, e_s, is fixed in each of the stable sets. For the ERTBP, the same true anomaly of Mars is chosen as the initial. The initial condition of the spacecraft corresponds to periapsis with respect to Mars. Two more parameters are used in the stable sets, the periapsis distance r_p and the orientation angle θ, which is the angle between x-axis in the rotating frame and the Mars-Spacecraft line, as shown in Fig. 1. For convenience, the n-stable sets with fixed eccentricity of the spacecraft and initial true anomaly of Mars are noted as $W_n(f_{m0}, e_s)$. The complementary sets, n-unstable sets, are noted as $\bar{W}_n(f_{m0}, e_s)$.

The integral of motion can also be expressed by stable sets parmeters,

$$J_E(\tilde{r}_p, e_s, \theta, f_{m0}) = \frac{1}{1+e_m\cos f_{m0}}\left((\tilde{r}_p\cos\theta+1-\mu)^2+(\tilde{r}_p\sin\theta)^2+\frac{2(1-\mu)}{\sqrt{(\tilde{r}_p\cos\theta+1)^2+(\tilde{r}_p\sin\theta)^2}}+\frac{2\mu}{\tilde{r}_p}+\mu(1-\mu)\right)+v_p^2 \tag{3}$$

where $\tilde{r}_p$ is the instantaneous normalized periapsis distance at f_{m0} and v_p is the periapsis velocity in the rotating frame

$$v_p = \sqrt{\frac{\mu(1+e_s)}{\tilde{r}_p}} - \tilde{r}_p \tag{4}$$

If we use the superscript ^{i} to represent the initial moment and the superscript ^{f} to represent the periareion moment after several revolutions, $f_{m0} = f_m^i$. The integral of motion J_E should satisfy

$$J_E^i(\tilde{r}_p^i, e_s^i, \theta^i, f_{m0}) = J_E^f(\tilde{r}_p^f, e_s^f, \theta^f, f_{m0}, f_m^f) \tag{5}$$

Due to the integral term in Eq. (2), there is no explicit solution for Eq. (5). The special case $e_m = 0$ is investigated, which corresponding to the circular problem. Equation (5) can be written as

$$\Omega_s^f + \frac{\mu(1+e_s^f)}{\tilde{r}_p^f} - 2\sqrt{\mu\tilde{r}_p^f(1+e_s^f)} + (\tilde{r}_p^f)^2 - J_C^i = 0 \tag{6}$$

where

$$\Omega_s^f = (\tilde{r}_p^f\cos\theta^f+1-\mu)^2+(\tilde{r}_p^f\sin\theta^f)^2+\frac{2(1-\mu)}{\sqrt{(\tilde{r}_p^f\cos\theta^f+1)^2+(\tilde{r}_p^f\sin\theta^f)^2}}+\frac{2\mu}{\tilde{r}_p^f}+\mu(1-\mu)$$

$$J_C^i = (\tilde{r}_p^i\cos\theta^i+1-\mu)^2+(\tilde{r}_p^i\sin\theta^i)^2+\frac{2(1-\mu)}{\sqrt{(\tilde{r}_p^i\cos\theta^i+1)^2+(\tilde{r}_p^i\sin\theta^i)^2}}+\frac{2\mu}{\tilde{r}_p^i}+\mu(1-\mu)+\frac{\mu(1+e_s^i)}{\tilde{r}_p^i}-2\sqrt{\mu\tilde{r}_p^i(1+e_s^i)}+(\tilde{r}_p^i)^2$$

Equation (6) can be considered as the quadratic equation for $\kappa = \sqrt{1+e_s^f}(\kappa > 0)$. That means, for a given integral constant J_C^i and periapsis parameters $(\tilde{r}_p^f, \theta^f)$, we can find the eccentricity e_s^f of the trajectory at the periphrasis by Eq. (6). Though there are two solutions for Eq. (6) mathematically, only one solution is valid $(\kappa > 0, e_s > 0)$ as,

$$e_s^f = \frac{4\mu(\tilde{r}_p^f)^3 + 4\sqrt{\mu(\tilde{r}_p^f)^5\Delta} - \Delta\,(\tilde{r}_p^f)^2}{4\mu^2} - 1 \tag{7}$$

where $\Delta = 4\mu\tilde{r}_p^f - 4\frac{\mu}{\tilde{r}_p^f}[\Omega_s^f + (\tilde{r}_p^f)^2 - J_C^i]$.

The periapsis distance $\tilde{r}_p^f$ is much smaller than the relative distance between primaries. Therefore, the orientation angle θ has little impact on the eccentricity e_s^f and we can fix $\theta^i = 0, \theta^f = 0$ for convenience. Eq. (7) builds the relationship between the integral of motion J_C and the stable sets parameters e_s, r_p. If we choose J_C^i between $J_1 = 2.999103$ and $J_2 = 3.001030$, where J_1 is slightly smaller than the Jacobi constant for L_2 point in the CRTBP and J_2 is the integral of motion for an orbit with eccentricity $e_s = 0.95$ and periareion distance $r_p = 3589$ km (about 200 km above the surface of Mars) and the periareion distance r_p^f between 3509 km to 250000 km, the contour of the spacecraft's eccentricity e_s^f with respect to J_C^i and r_p^f is shown in Fig. 3.

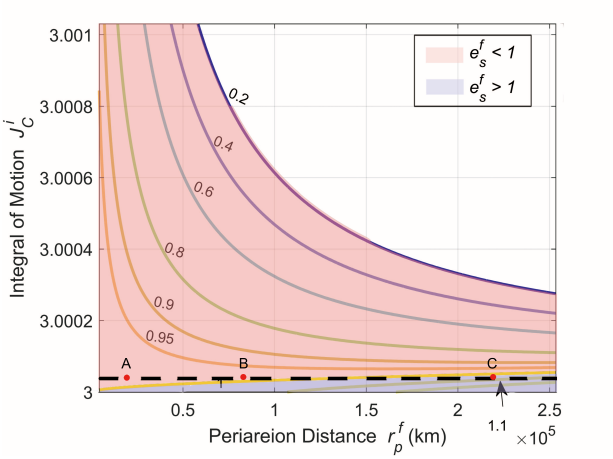

Fig. 3 Contour of the spacecraft's eccentricity with different integral constants and periareion distances

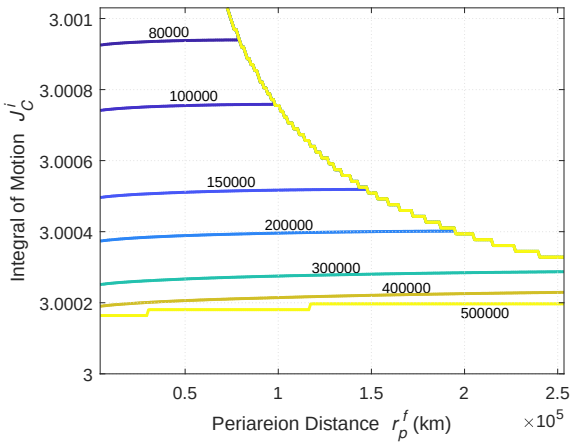

Fig. 4 Contour of the spacecraft's semi-major with different integral constants and periareion distances

For a given integral of motion $J_c^i(r_p^i, e_s^i)$, the periareion condition is available when $e_s^f > 0$. Here, the contour of eccentricity e_s^f from 0.2 to 1.1 are presented, which decreases with the increase of periareion distance and increases with the decrease of integral of motion. Besides, it is found that the eccentricity at the periareion may larger than 1 with a high periareion distance and low value of the integral of motion. According to the eccentricity of periapsis, the contour can be divided into two regions, $e_s^f > 1$ region and $e_s^f > 1$ region, marked in red and blue respectively in Fig. 3. As shown in Fig. 3, the available periareion distance exists in a narrow interval at a low energy level (large integral of motion). Decreasing J_C^i, the range of available periareion distance extends quickly and can cover the whole

region from 3589 km to above 250000 km. It is obvious that the initial periareion distance r_p^i is in the available area. According to the theory of three-body problem, the spacecraft may transfer between different states if they have the same integral of motion. That means it is possible that a low initial periareion r_p^i transfers to a high periareion naturally after several revolutions about Mars, as long as its initial integral of motion J_C^i is small.

We can also analyze Fig. 3 from the perspective of the stable sets. Define an initial state A locating in the $e_s^f < 1$ region. If its periapsis state transfers to $e_s^f > 1$ region after one turn about Mars, like point C in Fig. 3, the initial state A belongs to unstable sets. Trajectories will escape from Mars after those periapsides. On the contrary, if the periareion remains in $e_s^f < 1$ region after one turn about Mars, such as point B in Fig. 3, the initial state A belongs to stable sets. Although Fig. 3 can provide neither the specific transfer opportunity between two periareion states, nor the time of the transfer, it shows the possibility transfer between different periareion states and gives the ranges of periapsis distance with different energy levels theoretically, which can provide a new idea for the transfer or capture trajectory design.

Moreover, the semi-major axis of trajectories at periapsides is also shown in Fig. 4. For a fixed integral constant J_c^i, the semi-major axis increases with the increase of periapsis distance but the change rate is very small.

For the case of $e_m \neq 0$, the integral of motion contains the integral term related to the true anomaly of Mars f_m^i, f_m^f, which is hard to calculated analytically. Here an approximate analysis is given. It is found that Ω is bounded along a trajectory so long as it does not impact on the primaries or escape from the Sun-Mars system, which is satisfied in most cases. Therefore, the integral term in Eq. (2) should be bounded. The analogous equation of Eq. (6) can be established as.

$$\frac{\mu(1+e_s^f)}{\tilde{r}_p^f} - 2\sqrt{\mu\tilde{r}_p^f(1+e_s^f)} + \frac{\Omega_s^f}{1+e_m\cos f_m^f} - 2e_m\int_{f_{m0}}^{f_m^f}\frac{\Omega\sin\tilde{f}}{(1+e_m\cos\tilde{f})^2}d\tilde{f} + (\tilde{r}_p^f)^2 - J_E^i = 0 \tag{8}$$

Given an initial J_E^i and f_{m0}, and periapsis distance $\tilde{r}_p^f$, the eccentricity of the periareion should be bounded in a small interval. That means we can still find a feasible region of the periareion distance $\tilde{r}_p^f$ that satisfies $e_s^f > 0$. In that case, the potential transfer between different periareion states also exists in the ERTBP model, which has also been demonstrated numerically for the periodic orbits around Mars [30]. This property will be applied to design a new type of capture trajectory at Mars.

III. Methodology and Procedure

Normally, the ballistic transfer ends in a point $x_{p0}(r_{p0})$ in stable sets $W_n(e_s, f_{m0})$ $(n \geq 1)$ with a certain eccentricity e_s with respect to P_2. In [26], the beginning of the ballistic transfer is chosen far from Mars. From the view of stable sets, those trajectories come from -1-unstable set $\bar{W}_{-1}(e_s, f_{m0})$ and the capture points belong to the $e_s^f > 1$ regions in Fig. 3, where the periapsis distances tend to infinity. However, the complementary set -1-stable sets, $W_{-1}(e_s, f_{m0})$, or the trajectories with backward stability have not been used before.

We use the backward stable orbits for planetary capture. The capture trajectory starts from one of its periareion $x_{pc}(r_p^*)$ before it becomes unstable reversely. Those periapsides belong to the $e_s^f < 1$ regions in Fig. 3. Because a propulsive burn is required at the capture point, it is not exactly a ballistic capture. But the trajectory after the burn has some similar properties as the ballistic trajectory. We call it powered capture in the following part to distinguish it from the previous method [26].

There are several reasons to use the backward stable orbit and choose its periareion as the capture point. First, the backward stable orbits may have multiple periareion, which correspond to multiple capture opportunities to the same desired regions. Second, periareion of the orbit is close to Mars and within the Sphere of Influence (SOI) of Mars. In that case, any methods or techniques used in Earth-Mars transfer can be applied to the powered capture. Third, as shown in Fig. 3, the backward stable orbit may change its periapsis distance when its orbital energy is high, which may require less capture velocity increment. To be mentioned, the backward stable orbit might be temporary stable orbit. The orbit might escape from Mars or impact on the surface of Mars eventually, but the stable segment of the orbits are used for low-energy capture.

If it assumes the interplanetary trajectory has the Kepler energy $\varepsilon_1 > 0$ and the the backward stable orbit has the Kepler energy $\varepsilon_2 < 0$. The capture velocity increment at periareion is written as,

$$\Delta v = \sqrt{2\varepsilon_1 + \frac{2\mu_m}{r_p}} - \sqrt{2\varepsilon_2 + \frac{2\mu_m}{r_p}} \tag{9}$$

where r_p is the periareion distance and μ_m is the gravitational parameter of Mars.

Take the derivative of Δv with respect to the periareion distance r_p,

$$\frac{\partial \Delta v}{\partial r_p} = -\sqrt{\frac{\mu_m^2}{2r_p^3(\varepsilon_1 r_p + \mu_m)}} + \sqrt{\frac{\mu_m^2}{2r_p^3(\varepsilon_2 r_p + \mu_m)}} - \varepsilon_2' \sqrt{\frac{2r_p}{\varepsilon_2 r_p + \mu_m}} \tag{10}$$

where ε_2' is the change of ε_2 due to the periapsis distance. According to Fig. 4, ε_2' is relatively small and can be neglected. Hence, it gets $\frac{\partial \Delta v}{\partial r_p} > 0$ for arbitrary $r_p > 0$. The capture velocity increment Δv increases as r_p increases, which means the cost for capture will reduce, if it captures the spacecraft into a backward stable orbit at a lower periapsis distance.

According to the analysis above, the whole capture procedure to $W_n(e_s, f_{m0})$ can be described as follows. Instead of targeting the point x_{p0} in the stable set directly, the interplanetary trajectory will target the point x_{pc}, which is the lowest periapsis of the backward orbit from x_{p0}. Then, a capture maneuver Δv_c is performed at x_{pc} transferring the spacecraft from a interplanetary trajectory to a backward stable trajectory. Then the spacecraft will travel naturally from x_{pc} to x_{p0}. The capture is, in effect, accomplished when the spacecraft enters into the prescribed stable sets at x_{p0}. The sketch map of powered capture is shown in Fig. 5.

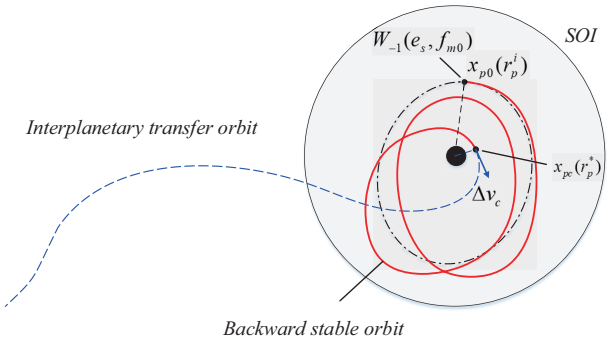

Fig. 5 Sketch map of powered capture

The key to designing powered capture is to find a periapsis $x_{pc}(r_p^*)$ satisfying $r_p^* < r_p^i$. The trajectories from the n-stable sets $W_n(e_s, f_{m0})$ are backward integrated with the same f_{m0} and e_s and their periareion distances are recorded. Special attention is made to those trajectories that have multiple periapsides. The periareion distances in each turn are compared and the lowest one is recorded as r_p^*. If the lowest periareion distance r_p^* is smaller than the initial value r_p^i, the periareion x_{pc} is selected as the capture point. That is to say, the segment of a trajectory from its lowest periareion $x_{pc}(r_p^*)$ to the initial point $x_{p0}(r_p^i)$ is used in powered capture. The spacecraft is captured at x_{pc} and the trajectory will naturally transfer to $x_{p0}(r_p^i)$ without extra maneuver. The powered capture requires the backward orbit has at least one periareion. To present the scope of application of our capture method, define the target sets as $\varpi_{-1}^n(e_s, f_{m0}) = W_{-1}(e_s, f_{m0}) \cap W_n(e_s, f_{m0})$. In the following parts, the properties of the powered capture are investigated in detail and the capture efficiency is evaluated.

IV. Capture Trajectories for Mars

A. Target sets for Mars

First of all, the geometric structure of target sets for Mars are discussed. Here we choose the target sets as the intersection of the 1-stable sets and the -1-stable sets to maximum the capture opportunity. Increasing the stability number of forward stable sets n will reduce the capture opportunity but obtain more robust trajectories after capture. The eccentricity of Mars is considered and the initial true anomaly of Mars f_{m0} is set as a variable. The initial periareion distance with respect to Mars for searching colorblacktarget sets, r_p, is selected from 3589 km to 30000 km with interval $\Delta r_1 = 100$ km and from 30000 km to 250000 km with interval $\Delta r_2 = 1000$ km. The orientation angle θ is set from 0° to 360° with interval $\Delta\theta = 1^\circ$.

In the meantime, the periareion distances of the backward integrated trajectories from target sets are analyzed. If we assume $\mathbf{r}_s$ and $\mathbf{v}_s$ as the position and velocity vectors of the trajectory in the rotating frame. The position and

velocity vectors relative to Mars are written as

$$\begin{cases} \mathbf{r}_{sm} = \mathbf{r}_s - \mathbf{r}_m \\ \mathbf{v}_{sm} = \mathbf{v}_s - \mathbf{v}_m + \mathbf{v}_c \end{cases} \tag{11}$$

where $\mathbf{v}_m = [\frac{e \sin f}{\sqrt{1-e^2}}, 0, 0]^T$ is the velocity vector of Mars in the rotating frame, and $\mathbf{v}_c = \omega' \times \mathbf{r}_{sm}$ is the velocity of the rotating frame. The periareion satisfies

$$\begin{cases} \mathbf{r}_{sm} \cdot \mathbf{v}_{sm} = 0 \\ \ddot{\mathbf{r}}_{sm} > 0 \end{cases} \tag{12}$$

The lowest periareion distance of each trajectory is recorded as $r_p^* = \min(r_{pk},\ k = 1, 2, ..., n)$, k is the number of the periareion passage. According to the periapsis distance, target sets are classified into two types, Type I, the backward stable orbit from target sets has a lower periareion distance than its initial state ($r_p^* < r_p^i$); Type II, the lowest periareion distance of the backward stable orbit is still larger than its initial state ($r_p^* \geq r_p^i$). According to the discussion in Sec. III, Type I points in target sets are suitable for backward stable sets capture.

Next, the influence of Mars position on target sets is investigated. The true anomaly of Mars determines the relative distance from Mars to the Sun, which changes the value of perturbation caused by the Sun and will influence the dynamic properties of ballistic trajectories. Two special conditions are considered, $f_{m0} = 0$, in which the Sun has the strongest perturbation, and $f_{m0} = \pi$, where the Sun has the weakest effect. The target sets for case $e_s = 0.99$ are shown in Fig. 6.

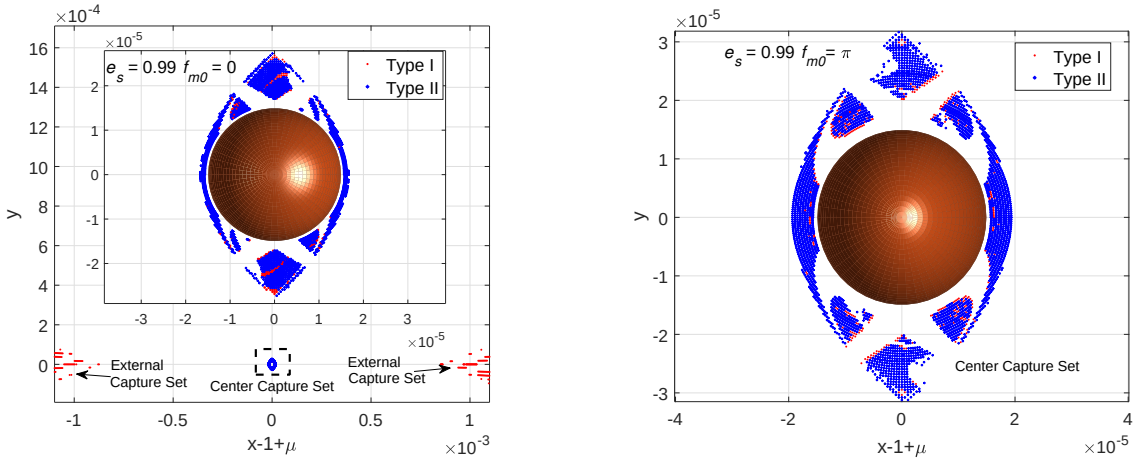

(a) Target sets at Mars perihelion $\varpi_{-1}^1(0.99, 0)$ **(b) Target sets at Mars aphelion $\varpi_{-1}^1(0.99, \pi)$**

Fig. 6 Target sets at Mars perihelion and aphelion with $e_s = 0.99$

As shown in Fig. 6, the target set at the perihelion of Mars ($f_{m0} = 0$) is different from that at the aphelion ($f_{m0} = \pi$). The target sets at aphelion only locates in the vicinity of Mars and are divided into several blocks by unstable sets. For convenience, we note the region as the center capture region. The structure of the center capture region is spindle-shaped, which has a larger extension along y-axis than x-axis. When Mars is at its perihelion, two more regions far from Mars appear, called the external capture regions. One of the external regions locates between Mars and the Sun, and the other lies at the outer side of Mars. Both regions are close to the x-axis. Considering the periareion distance, two types of target sets are marked in different notations in Fig. 6. Most of the points in the center capture region belong to Type II and only a few points close to the inner edge of blocks belong to Type I. On the contrary, all points in the external capture regions are Type I. All trajectories from those regions have at least one lower periareion than their initial states, which can be used for low-energy capture.

The eccentricity is an important parameter for the stable sets as well as the target sets, which affects the stability of corresponding backward trajectories. Hence, the target sets for smaller eccentricities are further investigated and illustrated in Fig. 7.

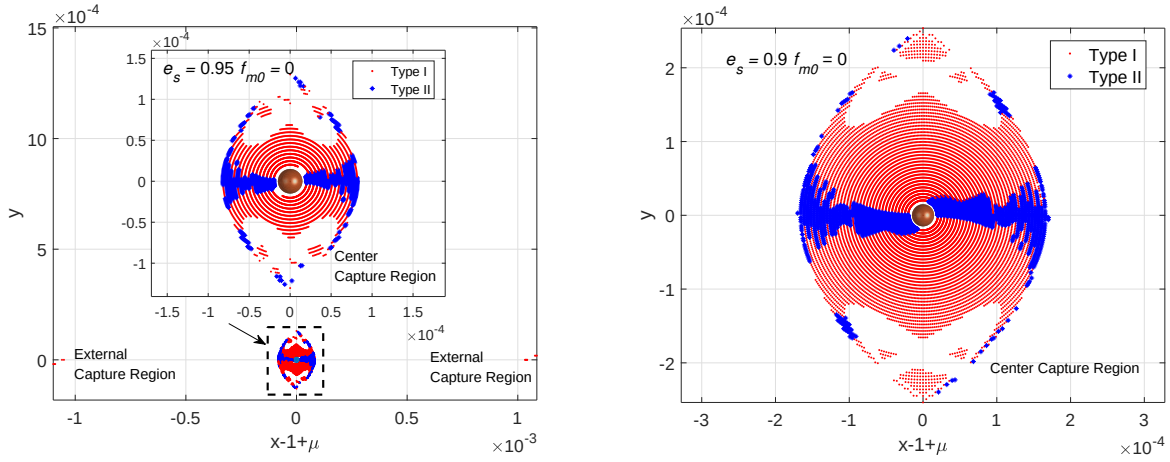

(a) $\varpi_{-1}^{1}(0.95, 0)$ **(b)** $\varpi_{-1}^{1}(0.90, 0)$

Fig. 7 Target sets for different eccentricities e

As shown in Fig. 7, the size of the center capture region increases as the eccentricity decreases and more points becomes Type I, which means more energy-saving capture opportunities appear. Type II points distribute in a stripe region close to x-axis and the outer edge of the target sets. The orientations θ of them are around 0 and 180 degrees. Furthermore, the two external regions gradually move away from Mars and finally disappear.

Compared with the previous ballistic capture method [26], it is important to note that by introducing the backward stable orbits, the region close to Mars can be employed in the backward stable set capture.

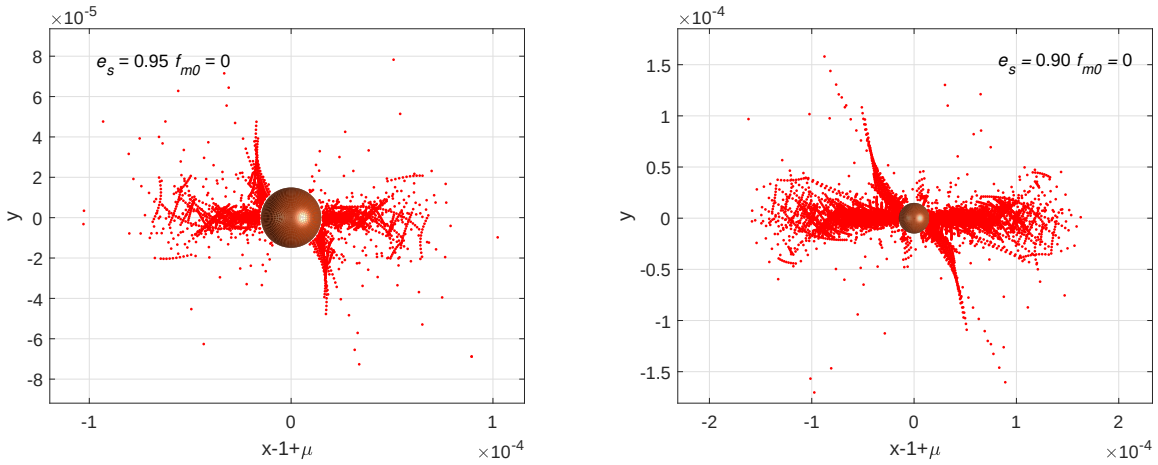

(a) Periareion for $\varpi^1_{-1}(0.95,0)$ **(b) Periareion for $\varpi^1_{-1}(0.90,0)$**

Fig. 8 Distribution of the lowest periareion of capture trajectories from target sets

B. Periareions of Capture Trajectories

According to Eq. (10), lower periareion distance requires less capture velocity increment. In that case, the distribution of the lowest periareion of each capture trajectory in Type I are of interest. Fig. 8 shows the result. In contrast to the initial target sets, the lowest periareion mainly locates along the x-axis. The orientations θ of most of periareions are between $[-68.72°, 18.91°]$ (here the periodicity of θ is used) and $[132.92°, 206.26°]$. No periareion distributes at $\theta = 90°$ and $270°$. Decreasing the eccentricity of the target set will extend the range of periareions along x-axis. Besides, the eccentricity of Mars has little influence on the distribution of periareions.

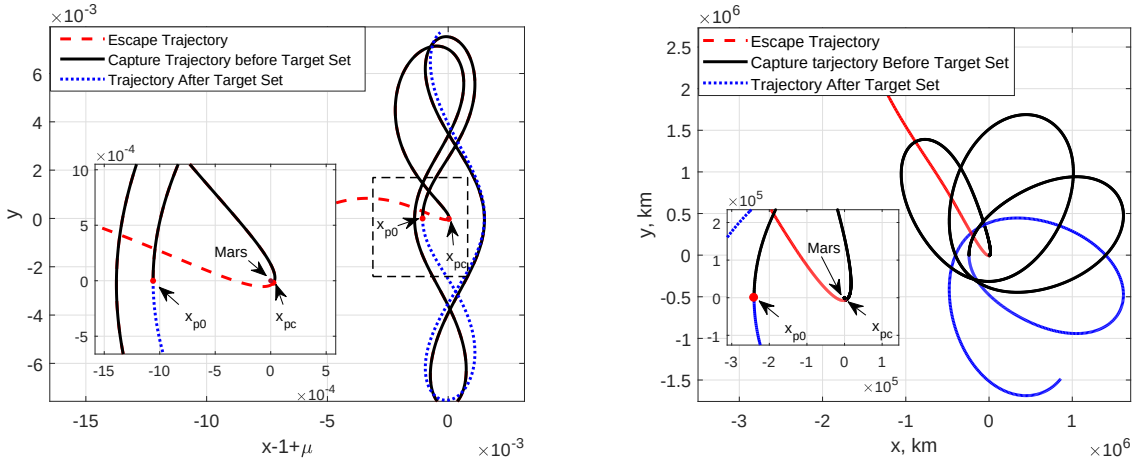

(a) Trajectory in the rotating frame **(b) Trajectory in the inertial frame**

Fig. 9 Capture trajectory from $\varpi^1_{-3}(0.95,0)$

Figures 9 and 10 show two capture trajectories from target sets before and after target sets in the rotating frame and the inertial frame, respectively. In Fig. 9, the trajectory comes from the external capture region in $\varpi^1_{-3}(0.95,0)$

and will backward escape from Mars after three cycles. Figure 10 shows a backward impact trajectory from the target sets $\varpi^1_{-2}(0.95,0)$. Figure 11 further shows the distance to Mars before and after target set in two cases and x_{pc} is the lowest periareion. Both the trajectories and distance diagrams shows that the periareion distance changes dramatically in each cycle. Though trajectory becomes unstable eventually, the stable segment from x_{pc} to x_{p0} can be used for the capture trajectory.

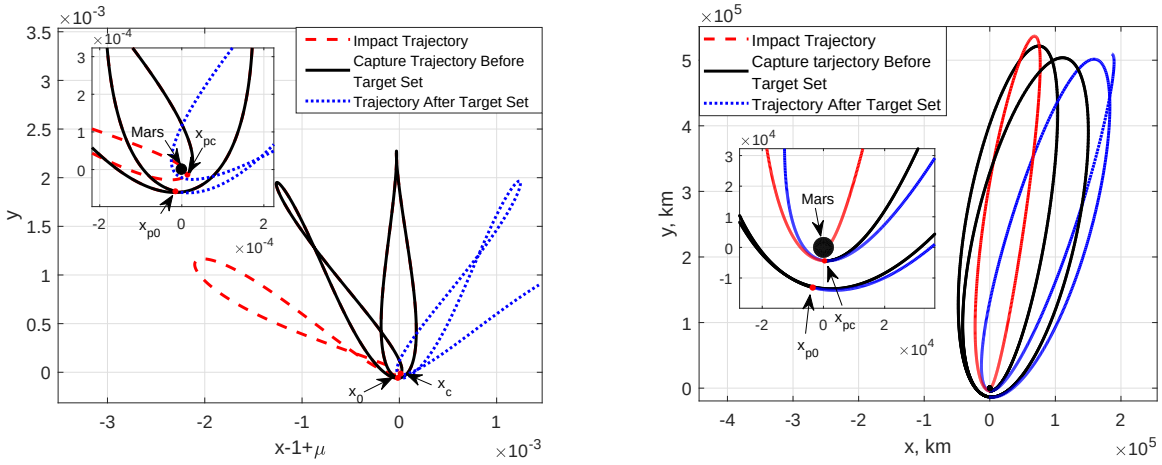

(a) Trajectory in the rotating frame **(b) Trajectory in the inertial frame**

Fig. 10 Capture trajectory from $\varpi^1_{-2}(0.95,0)$

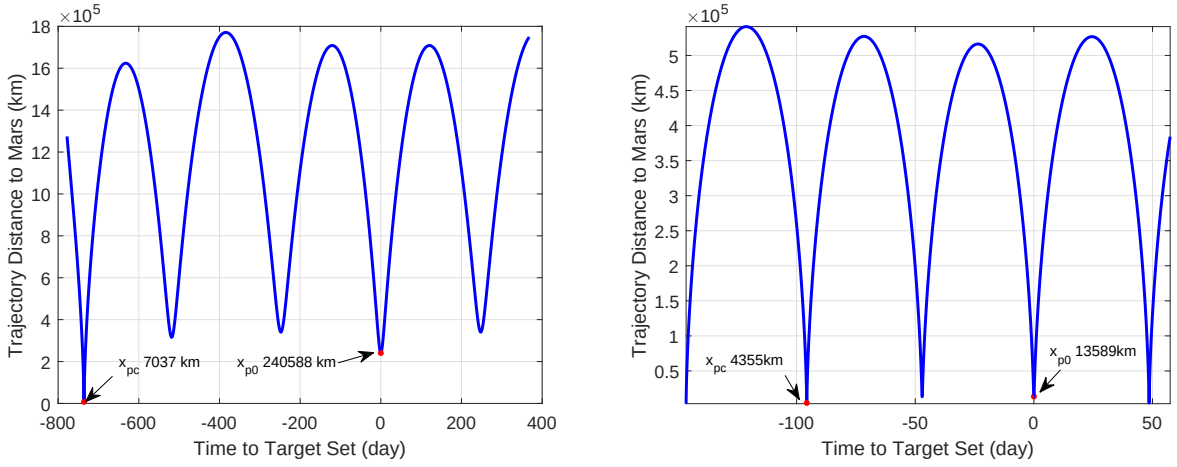

(a) Trajectory from $\varpi^1_{-3}(0.95,0)$ **(b) Trajectory from $\varpi^1_{-2}(0.95,0)$**

Fig. 11 Distance diagram for capture trajectories

The relationship between initial periareion distance r_p^i and the lowest periareion distance r_p^* is further investigated. The results are shown in Fig. 12, where each point corresponds to one pair of initial distance and orientation angle from the target sets $\varpi^1_{-1}(e_s, f_{m0})$. As shown in Fig. 12, the initial eccentricity e_s has a strong influence on the periareion distance of the backward stable orbits, especially for points from the center capture region. Besides,

different orientations θ in the target sets have different periareion distances r_p^*. As we fix the initial eccentricity in each case, the points with larger r_p^i have larger orbital energy (smaller integral of motion J). According to Fig. 4, the available periapsis distance range is wider. Meanwhile, those orbits have larger apoapsis distance, where the sun perturbation is stronger. In that case, the points in high initial distances are scattered.

If we pay attention to the minimum value of r_p^* for each initial distance r_p^i, defined as $r_{p\,\min}^* = \min\{r_p^*(r_p^i = r), r \in [3589, 250000]\,\text{km}\}$ (shown in red line in figures), it is found that $r_{p\,\min}^*$ is the function of both e_s and r_p^i. The trajectories near the edge of target sets have the same low periareion distance as those close to Mars, which implies that the transfer to low-altitude and high-altitude orbits may cost nearly the same propellant.

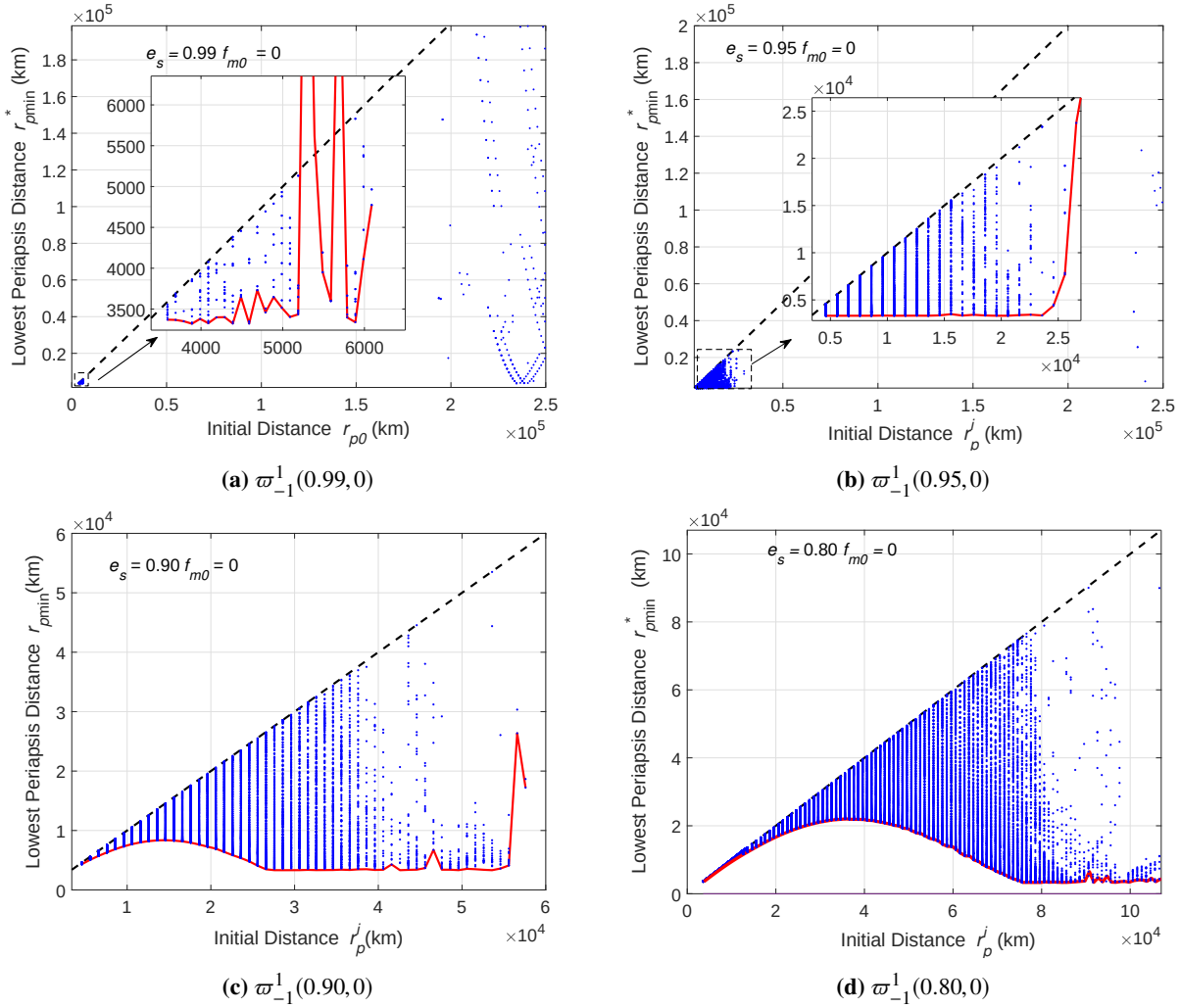

(a) $\varpi_{-1}^1(0.99, 0)$ **(b)** $\varpi_{-1}^1(0.95, 0)$

(c) $\varpi_{-1}^1(0.90, 0)$ **(d)** $\varpi_{-1}^1(0.80, 0)$

Fig. 12 Relationship between initial distance r_{p0} and the lowest periareion distance r_p^*

V. Performance of Powered Capture

In this section, the performance of powered capture is analyzed and compared with direct capture and the previous method in Ref. [26]. The cost for powered capture is computed under the following assumptions: 1). the whole transfer is planar, that is, the interplanetary trajectory is in the same plane as the ballistic orbit. 2). the periareion of the interplanetary trajectory with respect to Mars is equal to the periareion of a capture trajectory.

The capture maneuvers for powered capture and direct capture both occur in the Mars SOI. Therefore, we simplify the transfer from the Earth to Mars and concentrate on the excess velocity v_∞ at the Mars SOI. Assuming the velocity of capture trajectories at the capture point as v_p^*, the cost for powered capture is

$$\Delta v_c = \sqrt{v_\infty^2 + \frac{2\mu_m}{r_p^*}} - v_p^* \tag{13}$$

Here the gravitational parameter of Mars is set as $\mu_m = 4.2811 \times 10^4$ km^3/s^2. The trajectory will naturally go to the target sets $\varpi_{-1}^1(e_s, f_{m0})$ with the specific periareion radius r_p. The cost for direct orbit injection with the same eccentricity and periareion distance, following [31], is

$$\Delta v_d = \sqrt{v_\infty^2 + \frac{2\mu_m}{r_{p0}}} - \sqrt{\frac{\mu_m(1+e)}{r_{p0}}} \tag{14}$$

First, the performance of powered capture is assessed under different excess velocities in case of $v_\infty = 1.88$km/s and $v_\infty = 3.39$ km/s, which are the minimum and maximum excess velocity of bi-tangential transfers from Earth[26]. Type I target sets $\varpi_{-1}^1(0.99, 0)$ is chosen. The results are shown in Fig. 13, in which the black curves are the function of Δv_d. Several findings arise from the results. Consistent with the analysis above, almost all points in Type I target sets require less velocity increments than direct capture. For a fixed periareion distance and eccentricity, powered capture always exists better transfer opportunities than direct capture. Denote the minimum cost to a certain periareion r_p^i in $\varpi_{-1}^1(e_s, f_{m0})$ as $\Delta v_c^*(r_p^i, e_s, f_{m0})$. As shown in Fig. 13, for powered capture, the minimum cost $\Delta v_c^*(r_p^i, e_s, f_{m0})$ for different periareion distances are almost the same in such high eccentricity. In other words, using powered capture, the spacecraft can reach low altitude orbits and high altitude orbits with similar energy, which is different from direct capture.

Similar to direct capture, the cost of powered capture is also in relation to the excess velocity v_∞. However, the proposed capture method can save more energy than direct capture for a higher excess velocity, which means it is more efficient at higher excess velocity.

Next, capture is analyzed in low values of e_s. The excess velocity is fixed at $v_\infty = 3.39$ km/s. Figure 14 presents the results with different initial eccentricities $e_s = 0.95$, $e_s = 0.9$ and $e_s = 0.8$. As shown in Fig. 14, with the decrease of the eccentricity e, powered capture can be applied to high-altitude orbit capture, from about 6000 km at $e_s = 0.99$

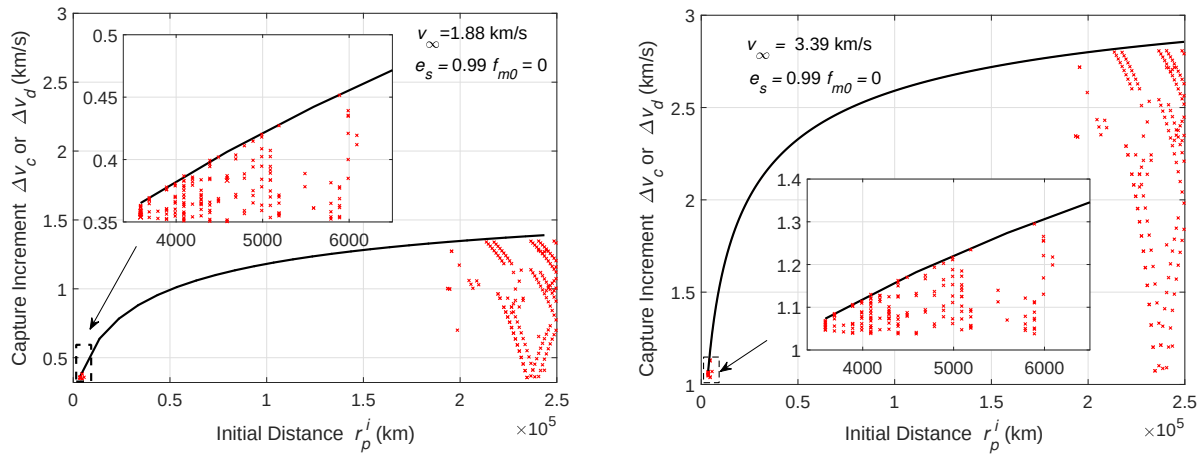

(a) v_∞ = 1.88 **km/s** **(b)** v_∞ = 3.39 **km/s**

Fig. 13 Comparison of direct capture and powered capture with different excess velocities

to more than 100000 km at $e_s = 0.8$. Besides the expansion of capture regions, the cost for capture also changes. In a low eccentricity, the minimum cost $\Delta v_c^*(r_p^i, e_s, f_{m0})$ is no longer the same for different distance r_p^i. With the increase of the initial distance, $\Delta v_c^*(r_p^i, e_s, f_{m0})$ increases at first and then decreases to a low level. It is interesting to note that, the minimum cost to a high-altitude orbit is even lower than to a low-altitude orbit, as illustrated in Fig. 9(b) and (c). That is a great advantage of powered capture compared with direct capture.

For a fixed periareion distance R_p, the powered capture by high-eccentricity target sets has the potential to save more fuel than by low-eccentricity target sets. For example, the minimum cost for distance $r_p^i = 30000$ km are $\Delta v_c^*(30000, 0.8, 0) = 2.004$ km/s and $\Delta v_c^*(30000, 0.9, 0) = 1.043$ km/s. Transfer to $\varpi_{-1}^1(0.9, 0)$ can save nearly 1 km/s velocity increment than to $\varpi_{-1}^1(0.8, 0)$. By contrast, the difference for direct capture is only 0.05 km/s ($\Delta v_d(30000, 0.8, 0) = 2.194$ km/s, $\Delta v_d(30000, 0.9, 0) = 2.150$ km/s).

Finally, the influence of Mars eccentricity is discussed. The cost of powered capture to the stable sets $e_s = 0.95$ at perihelion and aphelion are shown in Fig. 15. The excess velocity is set as $v_\infty = 2.09$ km/s. As illustrated in Fig. 15, the capture at aphelion can provide more opportunities for high-altitude orbit, but the minimum cost to the same distance does not change a lot.

Furthermore, if we compare our capture method (adopted -1-stable sets) with the method proposed in Ref. [26] (adopted -1-unstable set), several differences are noted. Firstly, the proposed method could provide more capture opportunities near Mars, especially in a low value of e_s, at the cost of fewer chances far from Mars. Secondly, the proposed method doesn't require extra the launch windows search and the traditional Earth-Mars launch windows can be used directly. But they cannot widen the launch windows as the previous method does. Thirdly, by utilizing the backward stable orbits, the proposed method can exploit the segment of escape trajectories, impact trajectories as well as long-term stable orbits as the capture trajectories.

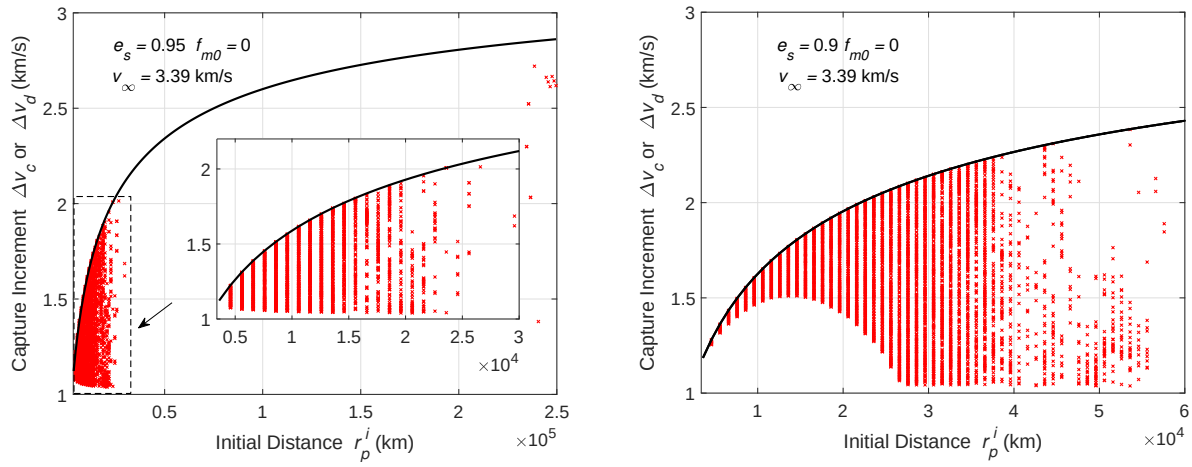

(a) $\varpi_{-1}^{1}(0.95, 0)$

(b) $\varpi_{-1}^{1}(0.90, 0)$

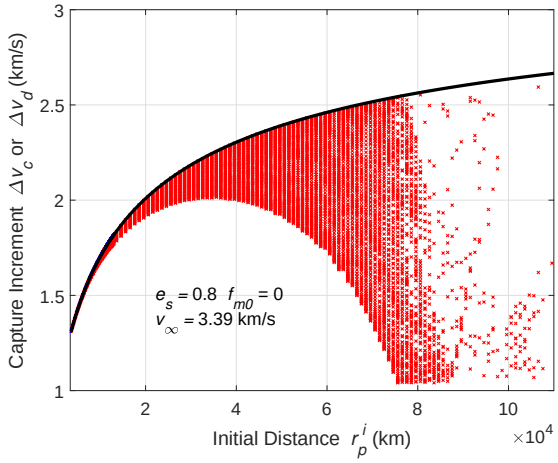

(c) $\varpi_{-1}^{1}(0.80, 0)$

Fig. 14 Comparison of direct capture and powered capture by different target sets

Besides, though the powered capture cannot find the capture opportunity to stable sets with large perihelion distances and a high eccentricity like the ballistic capture does, we can lower the eccentricity to find capture trajectories to similar orbit states (the same r_p and stability) with possible less velocity increment. For example, the ballistic capture to the stable set $W_6(46000, 0.99)$ needs about 2.09 km/s, while the minimum velocity increment to the stable sets $W_6(46000, 0.9)$ is 1.09 km/s for the backward stable set capture. Actually, for the same r_p, various backward stable orbits with different eccentricities can be used as capture trajectories, which also shows the flexibility of the powered capture.

VI. Conclusion

A novel energy-saving capture at Mars has been developed by using the backward stable orbits. The segment of a backward stable orbit from its lowest periareion to the desired periareion in the stable sets are used for capturing.

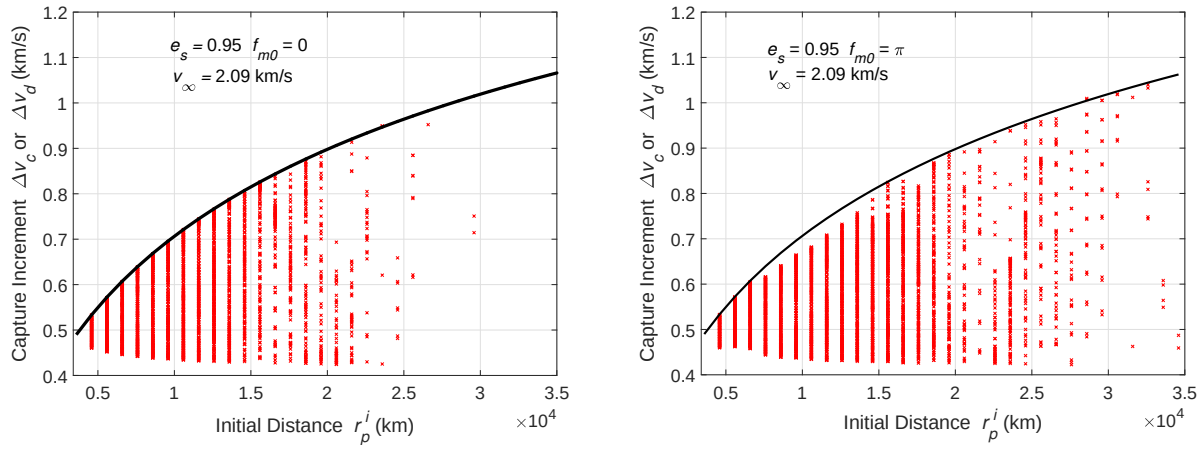

(a) $\varpi_{-1}^{1}(0.95, 0)$ **(b)** $\varpi_{-1}^{1}(0.95, \pi)$

Fig. 15 Influence of Mars eccentricity on powered capture

A capture maneuver is implemented at the periareion to send the spacecraft naturally to the stable sets. It is found that the capture cost will decrease if the capture periareion is lower than the desired periareion in stable sets. The potential capture opportunities are investigated under different eccentricities e_s with respect to Mars and true anomaly of Mars f_{m0}, and the efficiency of proposed capture method is compared with different capture methods. Numerical results show that capture via backward stable orbits has great advantages on propellant saving especially for high-excess velocity and high-altitudes orbit transfer. It also provides more capture opportunities in the vicinity of Mars.

Acknowledgments

This work was supported by the National Natural Science Foundation of China (Grant No. 11572038 and No. 11772050), Chang Jiang Scholars Program, the Discipline Innovative Engineering Plan (111 Project) and Graduate Technological Innovation Project of Beijing Institute of Technology.

References

[1] Belbruno, E. A., and Miller, J. K., "Sun-perturbed Earth-to-Moon Transfers with Ballistic Capture," *Journal of Guidance, Control, and Dynamics*, Vol. 16, 1993, pp. 770–770. doi:10.2514/3.21079.

[2] Chung, M., Hatch, S. J., Kangas, J. A., Long, S. M., Roncoli, R. B., and Sweetser, T. H., "Trans-Lunar Cruise Trajectory Design of GRAIL (Gravity Recovery and Interior Laboratory) Mission," *AIAA/AAS Astrodynamics Specialist Conference*, Toronto, Ontario Canada, 2010.

[3] Belbruno, E., and Miller, J., "A Ballistic Lunar Capture Trajectory for the Japanese Spacecraft Hiten," *Jet Propulsion Laboratory, IOM*, Vol. 312, 1990, pp. 90–4.

[4] Circi, C., and Teofilatto, P., "On the Dynamics of Weak Stability Boundary Lunar Transfers," *Celestial Mechanics and Dynamical Astronomy*, Vol. 79, No. 1, 2001, pp. 41–72. doi:10.1023/A:1011153610564.

[5] Belbruno, E., *Capture Dynamics and Chaotic Motions in Celestial Mechanics: With Applications to the Construction of Low Energy Transfers*, Princeton University Press, 2004.

[6] Romagnoli, D., and Circi, C., "Earth–Moon Weak Stability Boundaries in the Restricted Three and Four Body Problem," *Celestial Mechanics and Dynamical Astronomy*, Vol. 103, No. 1, 2009, pp. 79–103. doi:10.1007/s10569-008-9169-y.

[7] García, F., and Gómez, G., "A Note on Weak Stability Boundaries," *Celestial Mechanics and Dynamical Astronomy*, Vol. 97, No. 2, 2007, pp. 87–100. doi:10.1007/s10569-006-9053-6.

[8] Topputo, F., and Belbruno, E., "Computation of Weak Stability Boundaries: Sun–Jupiter System," *Celestial Mechanics and Dynamical Astronomy*, Vol. 105, 2009, pp. 3–17. doi:10.1007/s10569-009-9222-5.

[9] Hyeraci, N., and Topputo, F., "Method to Design Ballistic Capture in the Elliptic Restricted Three-body Problem," *Journal of Guidance, Control, and Dynamics*, Vol. 33, No. 6, 2010, pp. 1814–1823. doi:10.2514/1.49263.

[10] Circi, C., "Properties of Transit Trajectory in the Restricted Three and Four-body Problem," *Advances in Space Research*, Vol. 49, No. 10, 2012, pp. 1506–1519. doi:10.1016/j.asr.2012.02.034.

[11] Fantino, E., Gómez, G., Masdemont, J., and Ren, Y., "A Note on Libration Point Orbits, Temporary Capture and Low-energy Transfers," *Acta Astronautica*, Vol. 67, No. 9-10, 2010, pp. 1038–1052. doi:10.1016/j.actaastro.2010.06.037.

[12] Belbruno, E., Gidea, M., and Topputo, F., "Weak Stability Boundary and Invariant Manifolds," *SIAM Journal on Applied Dynamical Systems*, Vol. 9, No. 3, 2010, pp. 1061–1089. doi:10.1137/090780638.

[13] Belbruno, E., Gidea, M., and Topputo, F., "Geometry of Weak Stability Boundaries," *Qualitative Theory of Dynamical Systems*, Vol. 12, No. 1, 2013, pp. 53–66. doi:10.1007/s12346-012-0069-x.

[14] Parker, J. S., Anderson, R. L., and Peterson, A., "Surveying Ballistic Transfers to Low Lunar Orbit," *Journal of Guidance, Control, and Dynamics*, Vol. 36, No. 5, 2013, pp. 1501–1511. doi:10.2514/1.55661.

[15] Luo, Z.-F., and Topputo, F., "Capability of Satellite-aided Ballistic Capture," *Communications in Nonlinear Science and Numerical Simulation*, Vol. 48, 2017, pp. 211–223. doi:10.1016/j.cnsns.2016.12.021.

[16] Oshima, K., Topputo, F., Campagnola, S., and Yanao, T., "Analysis of Medium-energy Transfers to the Moon," *Celestial Mechanics and Dynamical Astronomy*, Vol. 127, No. 3, 2017, pp. 285–300. doi:10.1007/s10569-016-9727-7.

[17] Campagnola, S., Buffington, B. B., and Petropoulos, A. E., "Jovian Tour Design for Orbiter and Lander Missions to Europa," *Acta Astronautica*, Vol. 100, 2014, pp. 68–81. doi:10.1016/j.actaastro.2014.02.005.

[18] Brasil, P., Prado, A., Deienno, R., and Yokoyama, T., "Study of the Gravitational Capture of a Spacecraft by Jupiter," *Advances in Space Research*, Vol. 55, No. 2, 2015, pp. 668–681. doi:10.1016/j.asr.2014.11.005.

[19] Campagnola, S., and Lo, M., "BepiColombo Gravitational Capture and the Elliptic Restricted Three-body Problem," *PAMM*, Vol. 7, No. 1, 2007, pp. 1030905–1030906. doi:10.1002/pamm.200700330.

[20] Hyeraci, Nicola, Topputo, and Francesco, "The role of true anomaly in ballistic capture," *Celestial Mechanics and Dynamical Astronomy*, Vol. 116, No. 2, 2013, pp. 175–193. doi:10.1007/s10569-013-9481-z.

[21] Luo, Z.-F., Topputo, F., Bernelli-Zazzera, F., and Tang, G.-J., "Constructing ballistic capture orbits in the real Solar System model," *Celestial Mechanics and Dynamical Astronomy*, Vol. 120, No. 4, 2014, pp. 433–450. doi:10.1007/s10569-014-9580-5.

[22] Mingotti, G., Topputo, F., and Bernelli-Zazzera, F., "Earth–Mars Transfers with Ballistic Escape and Low-thrust Capture," *Celestial Mechanics and Dynamical Astronomy*, Vol. 110, No. 2, 2011, pp. 169–188. doi:10.1007/s10569-011-9343-5.

[23] Topputo, F., Vasile, M., and Bernelli-Zazzera, F., "Low Energy Interplanetary Transfers Exploiting Invariant Manifolds of the Restricted Three-body Problem," *Journal of the Astronautical Sciences*, Vol. 53, No. 4, 2005, pp. 353–372.

[24] Luo, Z.-F., and Topputo, F., "Analysis of Ballistic Capture in Sun–planet Models," *Advances in Space Research*, Vol. 56, No. 6, 2015, pp. 1030–1041. doi:10.1016/j.asr.2015.05.042.

[25] Li, X., and Qiao, D., "Earth-Phobos Transfer with Ballistic Trajectory in the Sun-Mars System," *2018 AIAA SPACE and Astronautics Forum and Exposition*, 2018, p. 5309.

[26] Topputo, F., and Belbruno, E., "Earth–Mars Transfers with Ballistic Capture," *Celestial Mechanics and Dynamical Astronomy*, Vol. 121, No. 4, 2015, pp. 329–346. doi:10.1007/s10569-015-9605-8.

[27] Bertachini de Almeida Prado, A. F., "Close-approach Trajectories in the Elliptic Restricted Problem," *Journal of Guidance, Control, and Dynamics*, Vol. 20, No. 4, 1997, pp. 797–802. doi:10.2514/2.4115.

[28] Hiday-Johnston, L. A., and Howell, K. C., "Transfers between libration-point orbits in the elliptic restricted problem," *Acta Astronautica*, Vol. 32, No. 4, 1994, pp. 245–254. doi:10.1007/BF00692008.

[29] Campagnola, S., Lo, M., and Newton, P., "Subregions of Motion and Elliptic Halo Orbits in the Elliptic Restricted Three-Body Problem," *Spaceflight Mechanics: 18th AAS/AIAA Space Flight Mechanics Meeting*, Galveston, TX, 2008, pp. 08–200.

[30] Dei Tos, D. A., Russell, R. P., and Topputo, F., "Survey of Mars Ballistic Capture Trajectories Using Periodic Orbits as Generating Mechanisms," *Journal of Guidance, Control, and Dynamics*, Vol. 41, No. 6, 2018, pp. 1227–1242. doi: 10.2514/1.G003158.

[31] Nakamiya, M., Scheeres, D. J., Yamakawa, H., and Yoshikawa, M., "Analysis of Capture Trajectories into Periodic Orbits about Libration Points," *Journal of Guidance, Control, and Dynamics*, Vol. 31, No. 5, 2008, pp. 1344–1351. doi:10.2514/1.33796.